JOURNAL OF THE KOREAN ASTRONOMICAL SOCIETY
35: 97 ~ 103, 2002

CO OBSERVATIONS OF A HIGH LATITUDE CLOUD MBM 40 WITH A HIGH RESOLUTION AUTOCORRELATOR

YOUNGUNG LEE, HYUN SOO CHUNG, AND HYORYOUNG KIM
Korea Astronomy Observatory, Taeduk Radio Astronomy Observatory,
Whaam-dong 61-1, Yusong-gu, Taejon, 305-348, Korea
E-mail: yulee@trao.re.kr
(Received Mar. 7, 2002; Accepted Mar. 25, 2002)

ABSTRACT

We have mapped 1 deg^2 region toward a high latitude cloud MBM 40 in the $J = 1 - 0$ transition of ^{12}CO and ^{13}CO, using the 3 mm SIS receiver on the 14 m telescope at Taeduk Radio Astronomy Observatory. We used a high resolution autocorrelator to resolve extremely narrow CO linewidths of the molecular gas. Though the linewidth of the molecular gas is very narrow (FWHP < 1 km s^{-1}), it is found that there is an evident velocity difference between the middle upper part and the lower part of the cloud. Their spectra for both of ^{12}CO and ^{13}CO show blue wings, and the position-velocity map shows clear velocity difference of 0.4 km s^{-1}between two parts. The mean velocity of the cloud is 3.1 km s^{-1}. It is also found that the linewidths at the blueshifted region are broader than those of the rest of the cloud. We confirmed that the visual extinction is less than 3 magnitude, and the molecular gas is translucent. We discussed three mass estimates, and took a mass of 17 solar masses from CO integrated intensity using a conversion factor 2.3×10^{20} cm^{-2} (K km s^{-1})$^{-1}$. Spatial coincidence and close morphological similarity is found between the CO emission and dust far-infrared (FIR) emission. The ratio between the 100 μm intensity and CO integrated intensity of MBM 40 is 0.7 (MJy/sr)/(K km s^{-1}), which is larger than those of dark clouds, but much smaller than those of GMCs. The low ratio found for MBM 40 probably results from the absence of internal heating sources, or significant nearby external heating sources.

Key words: ISM: clouds — ISM: individual (MBM 40) — ISM: dust - ISM: molecules

I. INTRODUCTION

MBM 40 is a high latitude cloud (HLC), located at $(\alpha, \delta)_{1950} = (16^h09^m, +22°00')$, or $(l, b) = (37°.69, 44°.55)$, well isolated from the galactic plane. On the POSS (Palomar Observatory Sky Survey) plate, there is a weak, but clear nebulosity, which lead Sharpless (1959) to misidentify it as an HII region S73. One of the major privilege to study this cloud that it is without any background contamination problem. This HLC ensures relatively low line-of-sight extinction and avoids excessive line-of-sight superposition of dust clouds and crowding of the image by disk stars. Desert et al. (1988) included this cloud within their IR-excess clouds (IRECs) list as a cirrus cloud. As its visual extinction is less than 3 magnitude, MBM 40 is also a translucent cloud. While other cirrus clouds show widespread wispy and filamentary FIR emission features, it shows a well confined compact feature.

Molecular emission was first detected in this cloud by Blitz, Fich, & Stark (1982) during their CO survey toward HII regions, and this was just a single line observation. The first mapping toward this cloud was conducted by Magnani, Blitz, & Mundy (1985) during their high-latitude CO ($J = 1 - 0$) survey, however, the map was poorly sampled (on 10′ grid with a beam of 2′.3). From their survey the cloud is called as MBM 40. A first fully sampled map of MBM 40 was reported by de Vries (1988) in the CO ($J = 1 - 0$) survey transition with the Columbia 1.2 m Telescope (beamsize of 9′). Both the maps showed similar features, however, the resolution or sampling rate were not enough to analyze the detailed structure. Recently, Magnani et al. (1996) mapped the MBM 40 with a higher resolution. However, their observations were focused on the part of the central main ridge region, searching for the possible star formation, and the map was not for the whole region. They acclaimed that there were no evidence of recent or ongoing star formation through analysis of radio, infrared, optical, and X-ray data.

In this paper we present a first result of a high resolution observations of the whole extent of MBM 40 cloud with a high velocity resolution. We studied this cloud in $J = 1 - 0$ transition of ^{12}CO and ^{13}CO, and far-infrared data. Our major purpose at the first stage is to analyze the dynamics of gas component and correlation between gas and dust. Observational mode, far-infrared data and associated objects within the selected region are described in §II. In §III observational results along with physical parameters of the cloud are presented. In §IV we discuss the some highlights of the observational results, and the correlation between CO

Corresponding Author: Y. Lee

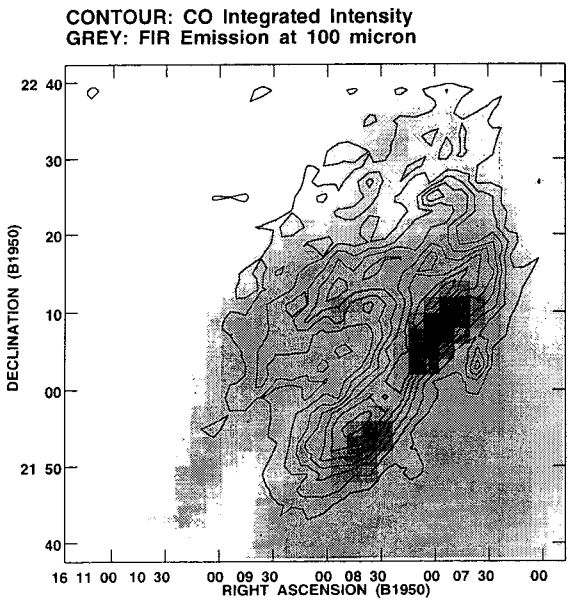

Fig. 1.— CO integrated intensity map overlayed on IRAS 100 micron image. Grey scale ranges from 3.0 to 11.5 MJy/ster, and the first contour is 1.5 K km s^{-1} and its increment is 1 K km s^{-1}.

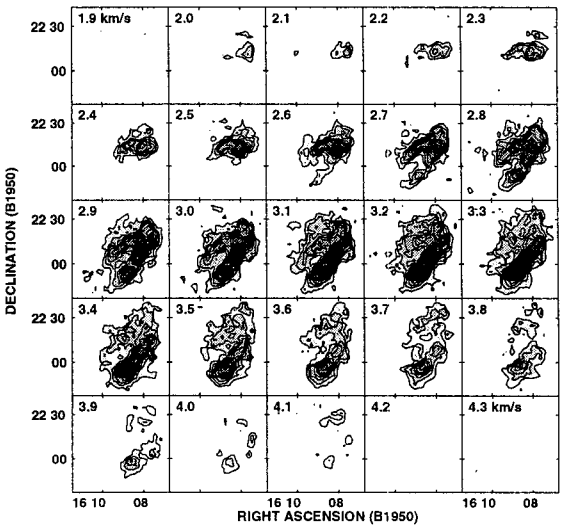

Fig. 2.— ^{12}CO velocity maps of MBM 40 molecular cloud. Each map has V_{LSR} step of 0.1 km s^{-1}. The contour levels are 1.5, 3, 5, and 8 K. The centered velocity of each map is marked at the middle upper-right corner of each panel.

emission and dust emission. We summarize our results in final section.

II. OBSERVATIONS AND IRAS DATA

We have mapped over 1 deg^2 region of whole extent of MBM 40 molecular cloud in ^{12}CO $J = 1 - 0$, and ^{13}CO $J = 1 - 0$, using the 3 mm SIS receiver on the 14 m telescope at Taeduk Radio Astronomy Observatory (TRAO). The observing grid is 2′ for the whole region. We used an autocorrelator with a resolution of 0.05 km s^{-1} per channel, and resampled the data with a resolution of 0.1 km s^{-1} to improve the noise level. The velocity range of the autocorrelator is 52 km s^{-1}. Nine hundred spectra for ^{12}CO and about 350 spectra for ^{13}CO were obtained. All observations were made by position switching between observed positions and reference positions which were carefully selected for free of CO emission. Calibration was accomplished by frequently observing an ambient temperature load. All antenna temperatures quoted are corrected for atmospheric extinction and for the forward spillover and scattering losses of the antenna and radome (η_{fss} = 0.63 at 110 to 115 GHz), and are therefore on the T_R^* temperature scale defined by Kutner and Ulich (1981). The average rms of the resampled spectra with 0.1 km s^{-1} is $\sim$ 0.5 K in T_R^*.

We have acquired 2 deg^2 IRAS Sky Survey Atlas image at 100 μm IRAS band centered on $(\alpha, \delta)_{1950}$ = $(16^h09^m, +22°00')$ from Infrared Processing and Analysis Center (IPAC) using Skyview Virtual Observatory (http://skyview.gsfc.nasa.gov/skyview.html), and examined the dust emission distribution of the region. Using an AIPS task HGEOM, we transforms IRAS image so that its geometry as described by the header is consistent with that of our CO map for comparison.

III. RESULTS

(a) CO Emission

The CO emission of MBM 40 is found to be well extended along the nebulosity surrounded. The CO emission integrated over all velocities, $\int T_R^* dV$, is presented in Figure 1. The peak temperature of 9 K in T_R^* arises at (α, δ) = $(16^h08^m19^s.3, 22°01'00'')$, while the brightest CO integrated intensity arises at (α, δ) = $(16^h08^m02^s.0, 22°11'00'')$. The morphology of the molecular gas is composed of a well developed main ridge distributed along NE-SW direction and more dispersed northern part. The overall structure is similar to a horse-shoe shape. Spatial coincidence and close morphological similarity is found between the CO emission and dust far-infrared (FIR) emission. The identification of dust emission would be straightforward if the clouds are well isolated. Correlation between CO emission and FIR dust emission of this region will be discussed in later section.

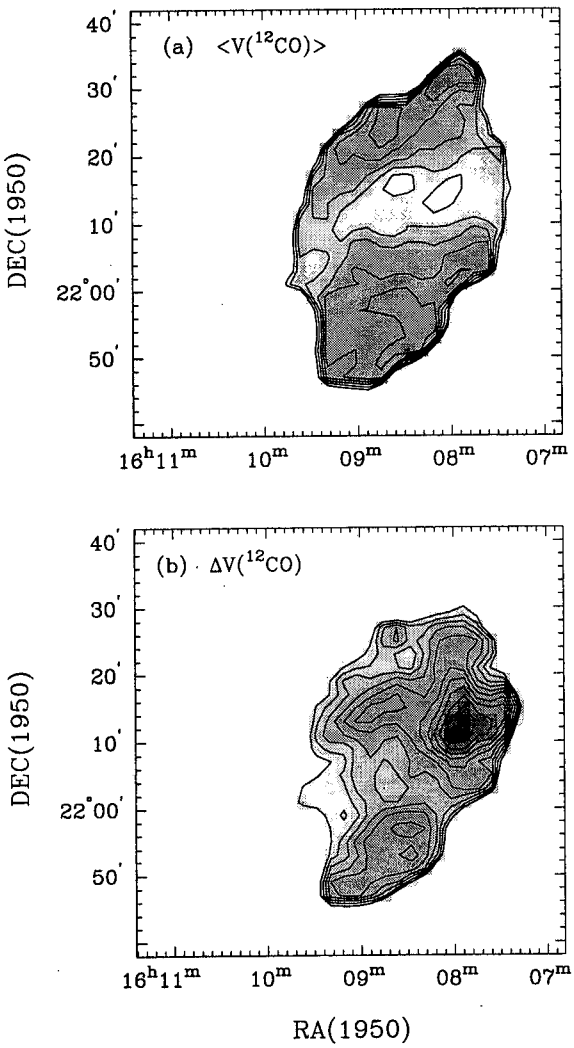

Fig. 3.— (a) Mean velocity map above a threshold larger than 3σ CO integrated intensity. Contour level is starting from 2.8 km s^{-1} and its increment is 0.1 km s^{-1}. (b) Linewidth map above a threshold larger than 3σ CO integrated intensity. The first contour is 0.7 km s^{-1}, and the contour increment is 0.05 km s^{-1}. The grey scale is ranging from 0.6 to 1.3 km s^{-1} .

(b) Velocity Field

The velocity of the cloud is well confined within a small range (from V_{LSR} = 2 to 4 km s^{-1}). The CO linewidth of the molecular gas are found to be extremely narrow (FWHP < 1 km s^{-1}), which is much smaller than those ($\sim$ 2 km s^{-1}) of local dark clouds. Though the linewidths are very narrow, it is found that there is apprehensible velocity gradient. The channel maps of the cloud is represented in Figure 2, and the center velocity of each panel is marked in 0.1 km s^{-1} step. Main ridge is conspicuous along the direction of northwest to southeast. The mean velocity of middle upper part of the cloud is around 2.8 km s^{-1} and that

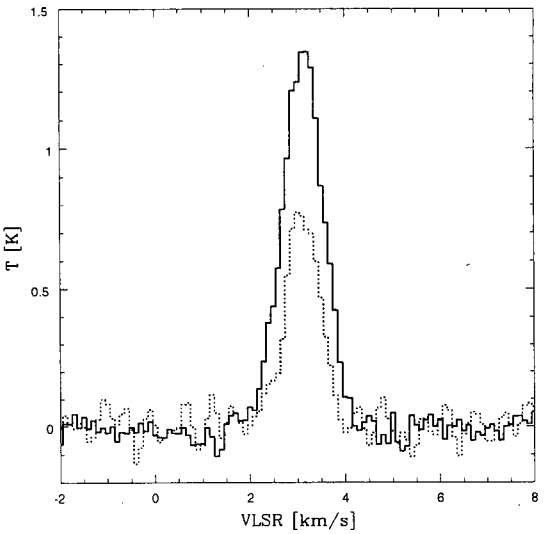

Fig. 4.— Average of the ^{12}CO (solid line) and ^{13}CO spectra (dashed line) of the whole region mapped. The ^{13}CO spectrum is multiplied by 5.

of lower part is 3.4 km s^{-1}. In Figure 3, mean velocity map and linewidth map are represented. We used a threshold-cutoff only for the meaningful region larger than the 3σ of the CO integrated intensity of the cloud. The mean velocity map represents that the velocity at the position of $(\alpha, \delta) = (16^h08^m00^s.0, 22°15'00'')$ is quite different from those of other part; the former part is more blueshifted than that of the rest part (Figure 3a). It is noticeable that the linewidths at the region with V_{LSR} < 2.8 km s^{-1} are broader than those of the rest (Figure 3b). These facts can be also confirmed with the average spectra of the whole region (Figure 4). Both of ^{12}CO and ^{13}CO averaged spectra centered on $(\alpha, \delta) = (16^h08^m00^s.0, 22°15'00'')$ are non-gaussian, and their blue-wing features are obvious at the velocity around 2.5 km s^{-1}, which is contributed mostly by the middle upper part of the cloud.

(c) Physical Parameters

To derive physical parameters of clouds, firstly, it is necessary to estimate linewidths and luminosities along with distance information. Distance to this cloud is established by Welty et al. (1989) as less than 150 pc, which is well consistent with the statistical estimate of the distance to the HLCs in general. Penprase (1993) has reestimated a distance of 90-140 pc with additional observations of the foreground stars. In this paper we adopt 100 pc as the distance to MBM 40 cloud. The cloud area is estimated to be about 1.1 pc^2 above a 3σ rms level of CO integrated intensity at this distance. We estimated ^{12}CO luminosity to be 3.26 K km s^{-1} pc^2, and ^{13}CO luminosity, 0.36 K km s^{-1} pc^2.

There are several ways to get the linewidth of a

cloud, and these have been discussed well in other papers (Lee 1994; Carpenter et al. 1990). We decompose gas motions within molecular clouds into two terms to get linewidths. The two motions had been discussed by Dickman & Kleiner (1985) and Lee et al. (1990). They represent two measurable motions within clouds: The first is an 'internal velocity dispersion' σ_i, which represents the spread of velocities observed along each line of sight, and second is a 'centroid velocity dispersion', σ_c, which is usually associated with point-to-point bulk motions of the gas within the cloud traced in a map. The centroid velocity dispersion is simply the ensemble variance of the line of sight average velocities. The internal velocity dispersion characterizes the magnitudes of gas motions along individual lines of sight with respect to the average velocities along those directions.

The total velocity dispersion of a cloud can be represented by $\sigma_{tot} = \sqrt{\sigma_i^2 + \sigma_c^2}$, and linewidth (FWHM) can be determined by $\Delta V_i = \sqrt{8\ln 2}\,\sigma_i$, assuming a Gaussian profile. We obtained the internal velocity dispersion to be 0.38 km s^{-1}, centroid velocity dispersion, 0.16 km s^{-1}. The total velocity dispersion is 0.41 km s^{-1}. The mean velocity is estimated to be 3.1 km s^{-1}.

The most frequently used way to estimate cloud mass is the relationship between the CO integrated intensity and molecular hydrogen column density or equivalently the relationship between CO luminosity and mass. The constant of proportionality then represents the conversion factor of CO luminosity or integrated intensity to mass or column density and implicitly assumes that such a factor has a general applicability. We have used an estimate of the conversion factor, 2.3×10^{20} cm^{-2} (K km s^{-1})$^{-1}$(Bloemen 1989), which has been established through γ-ray analysis. The estimated mass of MBM 40 using this conversion factor is 17 solar masses.

Another technique that can be used to estimate cloud masses is LTE method. When both ^{12}CO and ^{13}CO lines have been observed toward each line of sight, the ^{13}CO column density can be determined. We estimate optical depth and column density channel by channel with LTE assumption, constructing two cube (v, l, b) data for τ, and N(^{13}CO). The column density of ^{13}CO in the i-th pixel of a cloud is

$$\mathrm{N}(^{13}\mathrm{CO})_i = \frac{2.42 \times 10^{14} \Delta \mathrm{V}_i \, \mathrm{T_{ex}} \, \tau^{13}}{1 - \exp[-5.29/\mathrm{T_{ex}}]} \quad [\mathrm{cm}^{-2}], \quad (1)$$

where $\Delta \mathrm{V}_i = \sqrt{8\ln 2}\,\sigma_i^{13}$, and σ_i^{13} is defined in the same way as σ_i, and τ^{13} is line optical depth of ^{13}CO , The above equation was used for all the pixels with emission in ^{13}CO greater than a certain noise level ($3\sigma \sim 5\sigma$). For pixels with emission weaker than that noise level, we assumed optically thin emission and used the integrated intensity of ^{13}CO :

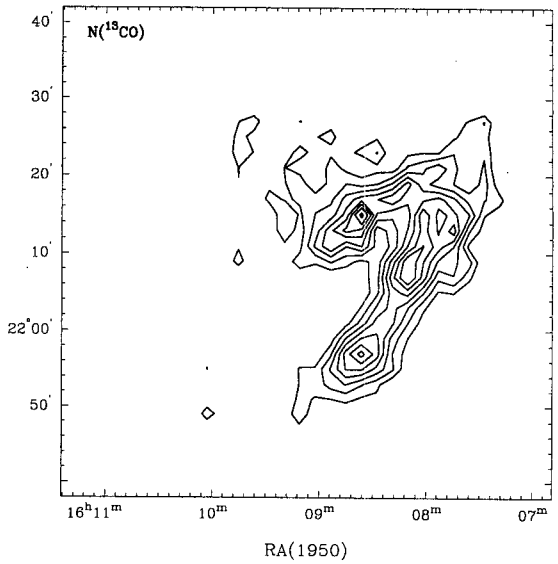

Fig. 5.— ^{13}CO column density map. Starting contour is 3×10^{14} cm^{-2}, and its increment is 2×10^{14} cm^{-2}.

$$N(^{13}CO)_i = \frac{3.76 \times 10^{14}}{f_u} \int T_R^*(^{13}CO)\, dv \quad [\mathrm{cm}^{-2}], \quad (2)$$

where f_u is the fraction of ^{13}CO in the upper state ($J = 1$), and it is depending on T_{ex}. Column density map is presented in Figure 5. This map is very similar to ^{13}CO integrated intensity map, thus we did not present it. The peak column density arise at $(\alpha, \delta)_{1950}$ = ($16^h08^m48^s$, +22°14′), about 2.5×10^{15} cm^{-2}. Assuming a $H_2/^{13}$CO abundance ratio of 5×10^5 (Dickman 1978) or 10^6, we can determine the H_2 column density and total mass. The visual extinction at the peak column density is estimated to be 2.6 magnitude. LTE masses derived in this manner have been multiplied by a factor of 1.36 to account for the contribution of He by mass. In this way, we obtained a mass of 7.4 solar masses for the target object.

If a molecular cloud is gravitationally bound, and has had enough time to be dynamically relaxed, then the partition of energy will be governed by the virial theorem, ignoring external pressure and magnetic field (Maloney 1988). This analysis is mostly applicable for giant molecular clouds with a few exceptions and globules, where the external pressure and magnetic field strength are negligible. Though the virial mass estimate may not be applicable to MBM 40, we estimated a virial mass of about 100 solar masses. The huge mass discrepancy will be discussed in later section.

(d) Dust Emission

The relationship between the dust emission in the infrared and the column density of CO in interstellar clouds deserves more study as both of the CO emis-

sion and the infrared emission from dust should be useful tracers of the distribution of mass within molecular clouds. Both of infrared continuum emission from dust and CO spectral line emission can be used to estimate the mass of interstellar clouds, and the FIR data can be compared for consistency and/or calibration with CO data. In fact, spatial coincidence and close morphological similarity is found between the CO emission for isolated clouds and their dust emission, especially after subtraction of the extended Galactic FIR emission (Heyer *et al.* 1987; Langer *et al.* 1989; and Mooney 1992). An accurate separation of the Galactic background FIR emission from the cloud emission is necessary to use the IRAS data to estimate the FIR luminosity of the cloud accurately. However, for the case of MBM 40 the identification of the FIR emission is straightforward as the cloud is well isolated.

The dust emission at 100 μm is very dispersed over the mapped region and obvious nebulosity is represented on POSS plate as described in Section 1. The size of the nebulosity is about 75′ (Blitz, Fich, and Stark 1982) and it shows a very intriguing feature; it has a shell-like structure with some dispersed filaments. Spatial coincidence and close morphological similarity is found between the CO emission and dust far-infrared (FIR) emission (see Figure 1), though there is partial displacement if we compare pixel to pixel, and lower boundary of FIR emission. These may be contributed from dispersed H I cloud.

A good correlation is found between the FIR emission and the ^{12}CO integrated intensity (Figure 6). Pixels with ^{12}CO integrated intensity above 1 K km s^{-1} have been fit by bisector least-squares (Lee 1992) to determine the relation between ^{12}CO integrated intensity and FIR flux. The equation of the fitted line is given below and illustrated in Figure 6:

$$I_{100} = 0.71(\pm 0.06) I_{^{12}CO} + 3.9(\pm 0.25) \qquad (3)$$

The non-zero intercept value most likely represents emission from dust of the region which is lack of ^{12}CO emission. The amount of dust that lies in front of or behind MBM 40, thus unassociated with the cloud, may be very small as the intercept of the above equation is non-negligible. However, if the intercept is from the contribution of dispersed H I gas, only the slope would represent the true relation between ^{12}CO integrated intensity and FIR intensity. The comparison of two correlationships between the FIR emission and the ^{12}CO integrated intensity will be discussed in later section.

IV. DISCUSSION

The linewidth of MBM 40 (σ_{tot} = 0.41 km s^{-1} and FWHP = 0.96 km s^{-1}) is much smaller than those (FWHP $\sim$ 2 km s^{-1}) of local dark clouds. Comparing with other MBM clouds' linewidths, which are ranging from σ_{tot} = 0.3 to 0.9 km s^{-1} (Gir et al. 1994), the linewidth of MBM 40 is on the very lower limit.

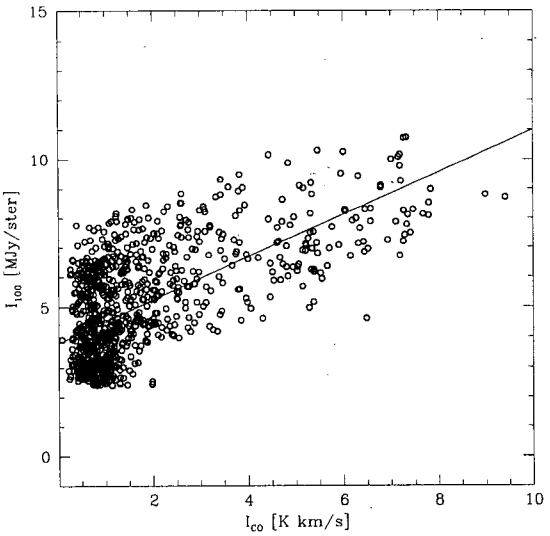

Fig. 6.— CO-IRAS pixel-to-pixel correlation.

Though the linewidth is very narrow, there is clear velocity gradient. Position-velocity map of the cloud (Figure 7) obviously shows the middle upper part is being shifted toward us, while the rest of the cloud is around the velocity = 3.3 km s^{-1}. The cloud is likely being distorted by non-uniform external pressure. There has been no report on the velocity gradient or field on MBM clouds. However, recent study of a dark cloud with narrow linewidth shows that there is similar velocity gradient on Lynds 694 cloud (Lee et al. 2002). Thus, detailed analysis based on high resolution observations can make a substantial contribution to the studies of the dynamic status of HLCs and dark clouds, and external pressure surrounding the molecular gas.

There is a big difference among three mass estimates. Virial mass estimate is based on the virial equilibrium, which assume a gravitational bound system, not including the external pressure. Thus, if the cloud is not gravitationally bound and internal turbulence is large, or the external pressure term becomes more significant, the virial mass would not be a proper estimate; The virial mass estimate of MBM 40 is a factor of 5.5 larger than mass estimate using CO integrated intensity. In the meanwhile, as ^{13}CO emission is weak, the LTE mass is substantially smaller than the other estimate (Lee 1994 and reference therein). Our mass estimate using a conversion factor can be compared with previous estimate by Magnani et al. (1996); They used a bit different conversion factor of 1.8×10^{20} cm^{-2} (K km s^{-1})$^{-1}$, and obtained 19 solar masses. They also attempted to estimate the cloud mass using the dust emission excluding H I contribution, and their estimate is about 40 solar masses (Magnani et al. 1996), which is over two times larger than our estimate. Taking their estimate, the current conversion factor should be cut down by a factor of 2. However, they did not discuss about

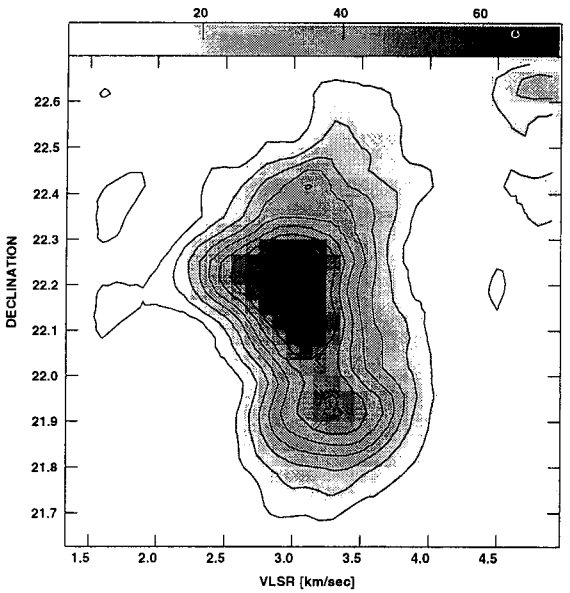

Fig. 7.— Position-velocity map of MBM 40. CO emission is integrated for the whole range of right ascension. The grey scale ranges from 1/60 to 11/60 K arcdeg. The lowest contour level and the increment between the levels are 2/75 K arcdeg, respectively.

substantial revision of conversion factor. There have been several studies concerning the universality of conversion factor, especially for the translucent clouds and GMCs in the external galaxies (Scoville and Sanders 1987; Bloemen 1989). This issue is still on the controversy and should remain to be seen. The mass of MBM 40 based on CO integrated intensity is likely more plausible within an error caused by the current conversion factor.

There have been several reports that there is a linear relationship between 100 μm intensity and total H (H I + H II) in molecular clouds (Boulanger & Pérault 1988; Snell, Heyer, & Schloerb, 1989). Recently, it has also been known that molecular gas of HLCs are correlated with H I distribution (Wouterloot et al. 2000 and reference therein). Though the atomic gas associated with molecular clouds can often contribute to the dust emission, especially for cirrus clouds, it does not always affect the slope of the CO column density-dust correlation since contribution to the slope of the H I to dust emission is very low (Lee et al. 1999) and the correlationship between H I and dust emission has a large dispersion. We did not include H I contribution to deduce a direct relationship between 100 μm and the CO column density in molecular clouds, as Gir et al. (1994) reported that there is relatively uniform H I distribution toward MBM 40 cloud.

Boulanger & Pérault (1988) found ratios between the 100 μm intensity and CO integrated intensity in the range 0.6 to 2.5 (MJy/sr)/(K km s^{-1}) with an average value of 1.4 (MJy/sr)/(K km s^{-1}) for regions outside of star forming sites. This value can be compared with the average slope found for MBM 40 of 0.7 (MJy/sr)/(K km s^{-1}), lower limit of star forming clouds. The slope can also be compared with those of non-star forming clouds: 0.36 of a cold, massive GMC G216-2.5, and 0.47 of Lynds 1251(Lee et al. 1999; Lee 1994). There has been no report on star forming activity in MBM 40 (Reach et al. 1995; Magnani et al. 1996), thus the higher slope of MBM 40 is quite noticeable. One possibility to heat up the cloud is external photons; as MBM 40 cloud is translucent with a visual extinction of less than 3 magnitude, and ionizing external photons can penetrate well into the cloud, and some of them will heat up the gas. Clear nebulosity around the MBM 40 could be another clue that the gas is being heated up by external source(s). Based on the slope of the least-squares fit to the data, we have computed the ratio of 100 μm intensity to total hydrogen column density. The CO conversion factor can be computed from the γ-ray analysis (Bloemen 1989), of 2.3×10^{20} H_2 cm^{-2} (K km s^{-1})$^{-1}$ to convert the CO intensities to hydrogen column densities. Expressing this ratio in terms of the hydrogen, the value is $I_{100\mu m}$/N(H) = 0.12 MJy/sr (10^{20} H cm^{-2})$^{-1}$. This value can be compared to those for dark clouds; $I_{100\mu m}$/N(H) is 0.07 for B18, and 0.10 for HCL2 (Snell, Heyer, & Schloerb 1989). The values for warmer GMCs are totally different; for example, in Orion: $I_{100\mu m}$/N(H) = 1.3 (Boulanger & Pérault 1988). The ratio found for MBM 40 is higher than the dark cloud ratios, but it is substantially smaller than the ratios in Orion. Snell, Heyer, & Schloerb (1989) attributed the low ratios in the dark clouds to dust heated exclusively by the solar neighborhood interstellar radiation field. Similar attribution can be applied to MBM 40 cloud, though slightly large excess of FIR leads Desert et al. (1988) to establish the IRECs. Recently Reach et al. (1998) conducted an extensive study of the IRECs, and acclaimed that these infrared excess clouds can be caused both by dust that is warmer than average or by dust associated with gas other than the atomic interstellar medium, however, infrared excess clouds are still cold. A similar conclusion was reached by Mooney (1992) for the clouds he classified as IR-quiet. Thus, the unusually low ratios found for dark clouds probably results from the absence of internal or significant nearby external heating sources. If this is not the case, the dust temperature should also be relatively higher than those of the dark clouds. Though MBM 40 is a bit higher ratio, the case would be similar to the dark clouds.

V. SUMMARY

We have mapped 1 deg^2 region toward a high latitude cloud MBM 40 in ^{12}CO ($J = 1 - 0$) and ^{13}CO ($J = 1 - 0$) to analyze the dynamics of gas component

and correlation between gas and dust. We used the 3 mm SIS receiver on the 14 m telescope at Taeduk Radio Astronomy Observatory. We used a high resolution (0.05 km s^{-1}) autocorrelator to resolve extremely narrow CO linewidths of the molecular gas. Though the linewidth of the molecular gas is very narrow (FWHP < 1 km s^{-1}), it is found that there is clear velocity difference between the middle upper part and the lower part of the cloud. Their spectra for both of ^{12}CO and ^{13}CO show blue wings, and the position-velocity map shows clear velocity difference of 0.4 km s^{-1}. The mean velocity of the cloud is 3.1 km s^{-1}. It is also found that the linewidths at the blueshifted region are broader than those of the rest of the cloud. We confirmed that the visual extinction is 2.6 magnitude, and that the cloud is translucent. We discussed all three mass estimates, and took a mass of 17 solar masses from CO integrated intensity using a conversion factor 2.3×10^{20} cm^{-2} (K km $s^{-1})^{-1}$. Spatial coincidence and close morphological similarity is found between the CO emission and dust far-infrared (FIR) emission. The ratio between the 100 μm intensity and CO integrated intensity of MBM 40 is 0.7 (MJy/sr)/(K km s^{-1}), which is larger than those of dark clouds, but much smaller than those of GMCs. The low ratio found for MBM 40 cloud probably results from the absence of internal or significant nearby external heating sources.

This work was supported by grant R01-2000-0025 from the Basic Research Program of the Korea Science and Engineering Foundation.

REFERENCES

Blitz, L., Fich, M., Stark, A.A. 1982, Catalog of CO Radial Velocities Toward Galactic H II Regions, ApJS, 49, 183.

Bloemen, H. J. B. G. M. 1989, Diffuse Galactic Gamma-ray Emission, ARA&A, 27, 469.

Boulanger F., and Pérault, M. 1988, Diffuse Infrared Emission from the Galaxy. I - Solar Neighborhood, 330, 964.

Carpenter, J. M., Snell, R. L., & Schloerb, F. P. 1990, Molecular Clouds Associated with Luminous Far-Infrared Sources in the Outer Galaxy, ApJ, 362, 147.

Desert, F. X., Bazell, D., Boulanger, F., 1988, An All-Sky Search for Molecular Cirrus Clouds, ApJ, 334, 815.

de Vries, H.M., 1988, High-Latitude Molecular Clouds and Infrared Cirrus, Ph.D. Dissertation, Columbia University, New York, NY, USA.

Dickman, R. L., Kleiner, S. C. 1985, Largescale Structure of the Taurus Molecular Complex - Part Three - Methods for Turbulence, ApJ, 295, 479.

Dickman, R. L. 1978, Star Counts and Visual Extinctions in Dark Nebulae, AJ, 83, 363.

Gir, Be-Young, Blitz, Leo, Magnani, L., 1994, The Associations of High-Latitude Molecular Clouds with H I Gas, ApJ, 434, 162.

Heyer, M. H., Vrba, F. J., Snell, R. L., Schloerb, F. P., Strom. S. E., Goldsmith, P. F., and Strom, K. M. 1987, The Magnetic Evolution of the Taurus Molecular Clouds. I - Large-Scale Properties, ApJ, 321, 855.

Kutner, M.L., Ulich, B.L., 1981, Recommendations for Calibration of Millimeter-Wavelength Spectral Line Data, ApJ, 250, 341.

Langer, W., Wilson, R. W., and Goldsmith P. F. 1989, Dust and Gas Emission Barnard 5, ApJ, 337, 355.

Lee, Y. 1992, Stucture and Star Forming Activities of the Cold Massive Molecular Cloud G216-2.5, Ph.D. Thesis, University of Massachusetts, Amherst, MA, USA.

Lee, Y., Snell, R.L., Dickman, R.L., 1990, Analysis of ^{12}CO and ^{13}CO Emission in a 3 Square Degree Region of the Galactic Plane between L=23 deg and 25 deg, ApJ, 355, 536.

Lee, Y. 1996, A Study of Lynds 1251 Dark Cloud: II. Infrared Properties, JKAS, 29(2), 107.

Lee, Y., Jung, J. H., Chung, H. S., Kim, H.-G., Park, Y.-S. Kim, H. R., Kim, B.-G., Kim, J., Han, S.-T. 1999, Galactic Anticenter CO Survey. I. Area l=178(deg) to 186(deg), b=3.5 to 6(deg), A&AS, 138, 187.

Lee, Y., Lee, C.W., Ryu, O.K., 2002, in preparation

Magnani L., Caillault J.-P., Hearty T., Stauffer J., Schmitt J. H. M. M., Neuhauser R., Verter F., & Dwek E. 1996, A Search for Star Formation in the Translucent cloud MBM 40, ApJ, 465, 825.

Magnani L., Blitz L., Mundy L., 1985, Molecular Gas at High Galactic Latitudes, ApJ, 295, 402.

Maloney, P. 1988, The Turbulent Interstellar Medium and Pressure-Bounded Molecular Clouds, ApJ, 334, 761.

Mooney, T. 1992, The Origin of the Far-Infrared Emission from Galactic Molecular Clouds, Ph.D. Dissertation, University of New York, Stony Brook

Penprase, B. E., 1993, Photometric and Spectroscopic Analysis of High Galactic Latitude Molecular Clouds. II - High-Resolution Spectroscopic Observations of NA I, CA II, CA I, CH, and CH^+, ApJS, 88, 433.

Reach, W.T., Pound, M.W., Wilner, D.J., and Lee, Y. 1995, Dense Gas in High-Latitude Molecular Clouds, ApJ 441, 244.

Reach, William T., Wall, William F., Odega, ApJ, 1998, Infrared Excess and Molecular Clouds: A Comparison of New Survey of Far-Infrared and H I 21 Centimeter Emission at High Galactic Latitudes, 507, 507.

Scoville, N. Z., and Sanders, D. B. 1987, H_2 in the Galaxy, in *Interstellar Processes*, eds. D. J. Hollenbach and H. A. Thronson, Jr., p. 21.

Sharpless, S. 1959, A Catalogue of H II Regions, ApJS, 4, 257.

Welty, D. E., Hobbs, L. M., Penprase, B. E., Blitz, L., 1989, On the Nearest Molecular Clouds. III - MBM 40, 53, 54, and 55, ApJ, 346, 232.

Wouterloot, J. G. A., Heithausen, A., Schreiber, W., Winnewisser, G., 2000, Multiline CO Observations of MBM 32, A&AS 144, 123.